RADIO EMISSION FROM SN 1994I IN NGC 5194 (M 51): THE BEST-STUDIED TYPE Ib/c RADIO SUPERNOVA

Citation: Weiler, Kurt W., Nino Panagia, Christopher Stockdale, Michael Rupen, Richard A. Sramek, and Christopher L. Williams. "RADIO EMISSION FROM SN 1994I IN NGC 5194 (M 51): THE BEST-STUDIED TYPE Ib/c RADIO SUPERNOVA." The Astrophysical Journal 740, no. 2 (October 3, 2011): 79. © 2011 The American Astronomical Society

As Published: http://dx.doi.org/10.1088/0004-637x/740/2/79

Publisher: IOP Publishing

Persistent URL: http://hdl.handle.net/1721.1/95632

Version: Final published version: final published article, as it appeared in a journal, conference proceedings, or other formally published context

RADIO EMISSION FROM SN 1994I IN NGC 5194 (M 51): THE BEST-STUDIED TYPE Ib/c RADIO SUPERNOVA

KURT W. WEILER[1], NINO PANAGIA[2,6], CHRISTOPHER STOCKDALE[3],
MICHAEL RUPEN[4], RICHARD A. SRAMEK[4], AND CHRISTOPHER L. WILLIAMS[5]

[1] Naval Research Laboratory, Code 7213, Washington, DC 20375-5320, USA; Kurt.Weiler@nrl.navy.mil
[2] Space Telescope Science Institute, Baltimore, MD 21218, USA; panagia@stsci.edu
[3] Physics Department, Marquette University, Milwaukee, WI 53201-1881, USA; Christopher.Stockdale@marquette.edu
[4] National Radio Astronomy Observatory, Socorro, NM 87801, USA; mrupen@nrao.edu, dsramek@nrao.edu
[5] MIT Kavli Institute for Astrophysics and Space Research, Cambridge, MA 02139, USA; clmw@mit.edu

ABSTRACT

We present the results of detailed monitoring of the radio emission from the Type Ic supernova SN 1994I from three days after optical discovery on 1994 March 31 until eight years later at age 2927 days on 2002 April 5. The data were mainly obtained using the Very Large Array at the five wavelengths of $\lambda\lambda 1.3$, 2.0, 3.6, 6.2, and 21 cm and from the Cambridge 5 km Ryle Telescope at $\lambda 2.0$ cm. Two additional measurements were obtained at millimeter wavelengths. This data set represents the most complete, multifrequency radio observations ever obtained for a Type Ib/c supernova. The radio emission evolves regularly in both time and frequency and is well described by established supernova emission/absorption models. It is the first radio supernova with sufficient data to show that it is clearly dominated by the effects of synchrotron self-absorption at early times.

Key words: galaxies: individual (NGC 5194 [M 51]) – radio continuum: stars – stars: mass-loss – supernovae: general – supernovae: individual (SN 1994I)

Online-only material: color figure

1. INTRODUCTION

1.1. Background

By 1941 Minkowski (1941) had recognized at least two classes of supernovae (SNe)—Type I with no hydrogen in their optical spectra and Type II with hydrogen lines in their optical spectra. By 1980 radio observations of supernovae began to play a role with the clear detection of SN 1979C (Weiler & Sramek 1980; there had been only one earlier detected radio supernova (RSN), SN 1970G, by Gottesman et al. 1972 and Goss et al. 1973 but the Westerbork telescope was unable to cleanly separate its radio emission from a nearby H II region) and the monitoring of its radio light curves at multiple radio frequencies for many years thereafter (Montes et al. 2000). The radio detection and monitoring of SN 1980K quickly followed (Weiler et al. 1986; Montes et al. 1998). However, both objects were optically identified as Type II SNe. At that time, little was known about the radio emission from SNe and the statistics with only two objects were very poor. However, the radio detection of SN 1983N (Sramek et al. 1984, also labeled SN 1983.51 by those authors), SN 1984L (Panagia et al. 1986), and SN 1990B (van Dyk et al. 1993) appeared to establish radio detections of Type I SNe. Around that time, Panagia et al. (1986) proposed that, from their optical spectra, Type I SNe were not a homogeneous class but split into at least two subclasses. The appearance of SN 1994I, the subject of this paper, finally yielded a bright, nearby object for detailed study of a "radio-loud" Type I supernova.

Currently, our understanding of the classes of SNe is such that the category of Type I supernovae is clearly bifurcated. One now speaks of Type Ia SNe (which still have never been detected in the radio; see Panagia et al. 2006) as originating in the deflagration of small stars, such as accreting or merging white dwarfs or black holes, and Type Ib/c and Type II SNe (of which there are also numerous subclasses) as originating in the core collapse of massive stars with a zero-age main sequence masses of $>8\ M_\odot$.

Particularly since the discovery of an association of SN 1998bw with GRB 980425 (Sadler et al. 1998), the study of Type Ib/c SNe has greatly increased (as explained below, the optical spectroscopic differences between Type Ib and Type Ic SNe are so slight that we treat them as a single class). However, further work has found that most Type Ib/c SNe ($\geqslant 97\%$) are not associated with detectable gamma-ray bursts (GRBs; Berger et al. 2003a; Soderberg et al. 2006).

Even with the enhanced study of Type Ib/c SNe since SN 1998bw, most are still relatively poorly sampled in the radio (see, e.g., Berger et al. 2003b; Soderberg et al. 2004, 2005, 2010) and, even at the present time, no Type Ib/c SN has been as thoroughly studied in the radio like SN 1994I presented in this paper.

1.2. SN 1994I

SN 1994I in M 51 (NGC 5194) was discovered at magnitude $V = 13\overset{\mathrm{m}}{.}5$ on 1994 April 2.17 UT (Puckett & Armstrong 1994) with independent discoveries by other observers following quickly (see IAUC 5961). Richmond & Filippenko (1994) confirmed the discovery as an SN and noted it as being "very blue." Armus & Mazzarella (1994) obtained moderate-dispersion spectra and noted "broad undulations superimposed on a generally featureless continuum."

Initial confusion arose as to the type identification of the SN with Schmidt & Kirshner (1994) first (incorrectly) identifying it as a Type II SN based on unreduced spectra taken by J. Peters and G. Bernstein during 1994 April 3.37–3.52 UT. The spectra, however, did suggest the SN location in NGC 5194

(M51) by identifying strong Na D lines at the recession velocity of the galaxy. By 1994 April 4.4 UT, Filippenko et al. (1994) suggested from new spectra that SN 1994I was a Type Ib SN. However, they noted the "possible presence of weak Hα" and suggested that, although the presence of hydrogen would "technically make it a Type IIb," the steep drop of the continuum toward the blue and near-ultraviolet was more consistent with a Type Ib identification, as were other aspects of the spectrum. Finally, Schmidt et al. (1994) confirmed that SN 1994I was not a Type II SN and Phillips (1994) pointed out the spectral similarities to the Type Ic SN 1983V. The Type Ic identification was also confirmed by Clocchiatti et al. (1994). (Note: because the spectral differences between the SN Type Ib and Type Ic optical classes are slight—Type Ib show strong He I absorption while Type Ic show weaker He I absorption—and there are no obvious radio differences, we shall hereafter refer to Type Ib/c SNe as one class.) Richmond (1994) discovered a red star near the SN position on *Hubble Space Telescope* (*HST*) Planetary Camera images from 1992 which he suggested as a possible progenitor to the SN, although his suggestion was disputed by Kirshner (1994).

On 1994 April 3.17 UT, Rupen et al. (1994) detected radio emission at the position of SN 1994I with the Very Large Array (VLA)[7] at both λ1.3 cm (22.4 GHz) and λ3.6 cm (8.4 GHz). The radio observations established an accurate position of R.A.(J2000) = $13^h29^m54\overset{s}{.}12$, decl.(J2000) = $+47°11'30\overset{''}{.}4$ with an uncertainty of $\pm 0\overset{''}{.}1$ in each coordinate with an offset from the radio nucleus of M 51 of $14\overset{''}{.}3$ east and $12\overset{''}{.}3$ south. Morrison & Argyle (1994) report a slightly different optical astrometric position of R.A.(J2000) = $13^h29^m54\overset{s}{.}072$, decl.(J2000) = $+47°11'30\overset{''}{.}50$ with uncertainty of $\pm 0\overset{''}{.}08$ in each coordinate, a difference of $\sim 0\overset{''}{.}5$ in R.A. and $\sim 0\overset{''}{.}1$ in decl. This optical/radio position difference might imply that there is a significant offset between the centroids of the optical and radio emission (unlikely since, at the distance of M51 at 8.9 Mpc; $0\overset{''}{.}5$ is 21.5 pc) or, more likely, that there is an offset between the radio reference frame and the FK5-based optical reference frame in that part of the sky. Tully (1988) determined a distance of 7.7 Mpc (assuming $H_0 = 75$ km s^{-1} Mpc^{-1}) to NGC 5194. Accepting the Tully (1988) method and using $H_0 = 65$ km s^{-1} Mpc^{-1}, we will adopt 8.9 Mpc as the distance to SN 1994I. Other distances to M51 range from 9.6 Mpc ($H_0 = 57$; derived from H II regions and brightest stars by Sandage & Tammann 1974) to 8.4 Mpc (Feldmeier et al. 1997) from planetary nebula luminosity.

Ultraviolet measurements were reported from the *International Ultraviolet Explorer* on 1994 April 3.35, 4.9, and 5.13 by Rodriguez-Pascual et al. (1994) and an infrared detection was reported on 1994 April 23.2 UT by Rudy & Dotan (1994) in the *J*, *H*, and 2.00–2.32 μm windows. An unabsorbed soft X-ray luminosity upper limit of $<1.5 \times 10^{38}$ erg s^{-1} for a distance to M51 of 7.7 Mpc was reported by Lewin et al. (1994) from the *ROSAT* satellite for 1994 May 22 and subsequent X-ray studies yielded the detection of SN 1994I with *ROSAT* at 82 days after explosion with $(1.82 \pm 4.2) \times 10^{38}$ erg s^{-1} (Immler et al. 1998). The *Chandra* X-ray Facility at 2271 and 2639 days after explosion reported $(1.4 \pm 0.7) \times 10^{37}$ erg s^{-1} and $(1.2 \pm 0.5) \times 10^{37}$ erg s^{-1}, respectively (Immler et al. 2002). Immler et al. (2002) determined a best-fit X-ray rate of decline proportional to t^{-1} and a circumstellar medium (CSM) density profile of $\rho_{CSM} \propto r^{-1.9\pm0.1}$, consistent at a constant

mass-loss rate/constant wind velocity for the SN progenitor which would yield a CSM density profile of $\rho_{CSM} \propto r^{-2}$.

Prediscovery limits are also available. Richmond et al. (1994) report that SN 1994I was not present to a limiting *R* magnitude of ~ 16.2 on 1994 March 28 UT and a prediscovery measurement with the VLA by Tongue et al. (1994) found a 3σ upper limit for λ21 cm emission from that position of <2.3 mJy on 1994 February 12.

Due to its proximity (8.9 Mpc; Tully 1988 recalculated for $H_0 = 65$ km s^{-1} Mpc^{-1}) and the fact that such an early radio detection was obtained, we quickly started observations at all available wavelengths with the VLA. Regular monitoring of SN 1994I with the VLA at λλ1.3 cm (22.5 GHz), 2 cm (14.9 GHz), 3.6 cm (8.4 GHz), 6 cm (4.9 GHz), and 20 cm (1.4 GHz) then continued until the end of 1994 with sporadic measurements thereafter. G. G. Pooley & D. A. Green (1994, private communication) also monitored the SN extensively at 2 cm (15.2 GHz) with the Ryle Telescope. These data are listed in Table 1. Two additional observations were taken with the Caltech Owens Valley Radio Observatory (OVRO) millimeter interferometer at 3 mm (99 GHz) and at 1.4 mm (218 GHz; Phillips et al. 1994). These are listed in Table 2.

2. RADIO OBSERVATIONS

2.1. Flux Density Measurements

The VLA radio observations reported here were made between 1994 April 3 and 2002 April 5. VLA phase and flux density calibration and data reduction followed standard procedures (see, e.g., Weiler et al. 1986, 1990), using 3C 286 as the primary flux density calibrator and J1418 + 546 as the secondary flux density and phase calibrator. As noted in the footnotes to Table 3, two measurements on 1994 April 3 used the calibrator J1415 + 463 and one measurement on 2002 April 5 used the calibrator J1327 + 434. Table 3 lists the measured or interpolated (or extrapolated) flux densities of the secondary calibrators. For the phase calibration, J1327 + 434, J1415 + 463, and J1418 + 546 have defined positions as listed in the NRAO VLA calibrator catalog.

The flux density measurements for SN 1994I are listed in Tables 1 and 2 and plotted in Figure 1 with the filled squares representing actual detections and inverted open triangles representing 3σ upper limits. Also shown in Figure 1 are the best-fit model curves discussed below in Sections 3 and 4 with the set of parameters reported in Table 4.

The flux density measurement error given for the VLA measurements in Table 1 is a combination of the rms map error, which measures the contribution of small unresolved fluctuations in the background emission and random map fluctuations due to receiver noise, and a basic fractional error ϵ included to account for the normal inaccuracy of VLA flux density calibration and possible deviations of the primary calibrator from an absolute flux density scale. These final errors (σ_f) are taken as

$$\sigma_f^2 = (\epsilon S_0)^2 + \sigma_0^2, \tag{1}$$

where S_0 is the measured flux density, σ_0 is the map rms for each observation, and $\epsilon = 0.10$ for 20 cm, $\epsilon = 0.05$ for 6 and 3.6 cm, $\epsilon = 0.075$ for 2 cm, and $\epsilon = 0.10$ for 1.2 cm. For all of the Cambridge measurements at 2 cm, $\epsilon = 0.10$ was assumed.

2.2. Spectral Indices

With such extensive data, we can also calculate the spectral index evolution for SN 1994I and these are shown in Figure 2

---

[7]   The VLA telescope of the National Radio Astronomy Observatory is operated by Associated Universities, Inc. under a cooperative agreement with the National Science Foundation.

Table 1
Centimeter Flux Density Measurements for SN 1994I

Obs. Date	Age (days)	Tel. Config.	S(20 cm) ± rms (mJy)	S(6 cm) ± rms (mJy)	S(3.6 cm) ± rms (mJy)	S(2 cm) ± rms (mJy)	S(1.3 cm) ± rms (mJy)
1994 Mar 31	= 0.00						
1994 Apr 3	3.167	VLA-A			0.554 ± 0.062		2.580 ± 0.388
1994 Apr 4	4.120	VLA-A			0.737 ± 0.120	2.780 ± 0.469	3.707 ± 0.891
1994 Apr 5	5.350	VLA-A	<0.090[a]	0.477 ± 0.091	1.743 ± 0.108	6.300 ± 0.522	8.299 ± 0.891
1994 Apr 6	6.040	VLA-A		0.700 ± 0.115			
1994 Apr 6	6.135	Camb				10.800 ± 1.472	
1994 Apr 6	6.483	VLA-A		1.400 ± 0.115			
1994 Apr 7	7.028	VLA-A			2.412 ± 0.152		
1994 Apr 7	7.070	VLA-A			3.295 ± 0.190		
1994 Apr 7	7.190	Camb				13.000 ± 2.385	
1994 Apr 7	7.462	VLA-A			3.656 ± 0.194	13.100 ± 1.062	16.300 ± 1.676
1994 Apr 8	8.020	Camb				14.500 ± 2.086	
1994 Apr 8	8.288	VLA-A	<0.207[a]	1.250 ± 0.153	4.990 ± 0.250	14.698 ± 1.202	15.458 ± 1.673
1994 Apr 9	9.180	Camb				16.000 ± 2.561	
1994 Apr 9	9.386	VLA-A		2.020 ± 0.144	6.514 ± 0.334	17.200 ± 1.409	17.100 ± 1.810
1994 Apr 10	10.561	VLA-A	<0.225[a]	2.123 ± 0.176	8.930 ± 0.455	19.171 ± 1.488	18.593 ± 2.028
1994 Apr 11	11.180	Camb				17.500 ± 2.658	
1994 Apr 12	12.180	Camb				17.200 ± 2.282	
1994 Apr 12	12.395	VLA-A	<0.132[a]	4.120 ± 0.221	11.43 ± 0.577	15.860 ± 1.249	12.400 ± 1.349
1994 Apr 13	13.220	Camb				13.900 ± 2.436	
1994 Apr 13	13.372	VLA-A	<0.162[a]	4.643 ± 0.271	12.605 ± 0.646	17.178 ± 1.365	12.610 ± 1.414
1994 Apr 14	14.220	Camb				15.600 ± 2.536	
1994 Apr 14	14.367	VLA-A	0.300 ± 0.067	5.053 ± 0.267	13.000 ± 0.660	16.500 ± 1.382	
1994 Apr 15	15.220	Camb				15.000 ± 2.500	
1994 Apr 15	15.360	VLA-A	<0.258[a]	5.587 ± 0.292	14.500 ± 0.733	16.500 ± 1.364	10.500 ± 1.178
1994 Apr 16	16.220	Camb				16.500 ± 2.593	
1994 Apr 16	16.356	VLA-A	0.370 ± 0.095	6.451 ± 0.338	16.200 ± 0.820	15.600 ± 1.236	11.000 ± 1.252
1994 Apr 17	17.210	Camb				16.100 ± 2.200	
1994 Apr 17	17.363	VLA-A	0.463 ± 0.105	7.664 ± 0.400	17.200 ± 0.871	16.900 ± 1.328	10.600 ± 1.185
1994 Apr 18	18.199	VLA-A		7.390 ± 0.392	15.770 ± 0.810	15.743 ± 1.215	10.590 ± 1.205
1994 Apr 18	18.210	Camb				15.900 ± 2.555	
1994 Apr 19	19.220	Camb				14.000 ± 2.441	
1994 Apr 20	20.200	Camb				13.500 ± 2.018	
1994 Apr 20	20.494	VLA-A	0.421 ± 0.107	9.250 ± 0.493	16.483 ± 0.850	8.757 ± 0.960	5.673 ± 1.185
1994 Apr 21	21.200	Camb				14.000 ± 2.052	
1994 Apr 22	22.210	Camb				13.000 ± 1.985	
1994 Apr 23	23.056	VLA-A	0.386 ± 0.089				
1994 Apr 23	23.150	Camb				12.000 ± 1.921	
1994 Apr 24	24.336	VLA-A	0.688 ± 0.125	11.130 ± 0.568			
1994 Apr 25	25.140	Camb				10.000 ± 1.414	
1994 Apr 25	25.333	VLA-A	0.720 ± 0.122	10.760 ± 0.551	12.300 ± 0.651		4.620 ± 0.816
1994 Apr 28	28.163	VLA-A	0.683 ± 0.115	13.713 ± 0.693	14.723 ± 0.760	7.503 ± 0.733	4.990 ± 0.706
1994 Apr 29	29.200	Camb				10.000 ± 1.281	
1994 Apr 30	30.320	VLA-A	1.618 ± 0.167	14.063 ± 0.726	14.650 ± 0.757	8.720 ± 0.848	6.293 ± 0.971
1994 May 2	32.140	Camb				9.800 ± 1.400	
1994 May 3	33.130	Camb				9.100 ± 1.212	
1994 May 3	33.279	VLA-BnA	1.170 ± 0.142	16.823 ± 0.847	11.440 ± 0.591		3.988 ± 0.624
1994 May 10	40.228	VLA-BnA	2.660 ± 0.267	17.550 ± 0.880	13.040 ± 0.656	5.330 ± 0.477	2.180 ± 0.555
1994 May 12	42.090	Camb				8.000 ± 1.281	
1994 May 15	45.179	VLA-BnA	2.470 ± 0.270	16.995 ± 0.861	12.788 ± 0.652	6.555 ± 0.615	3.533 ± 0.662
1994 May 16	46.100	Camb				8.000 ± 1.281	
1994 May 17	47.100	Camb				8.400 ± 1.306	
1994 May 19	49.252	VLA-BnA	3.420 ± 0.343	15.940 ± 0.798	11.040 ± 0.554	5.610 ± 0.523	2.810 ± 0.539
1994 May 23	53.208	VLA-BnA		15.860 ± 0.809	11.305 ± 0.570	5.380 ± 0.547	2.680 ± 0.722
1994 May 24	54.060	Camb				5.500 ± 1.141	
1994 May 27	57.060	Camb				5.500 ± 0.890	
1994 May 28	58.136	VLA-BnA	4.660 ± 0.466	14.030 ± 0.704	8.400 ± 0.425	4.240 ± 0.473	2.820 ± 0.645
1994 Jun 1	62.188	VLA-BnA	5.080 ± 0.508	12.400 ± 0.626	7.670 ± 0.392	3.390 ± 0.441	<2.250[a]
1994 Jun 17	78.165	VLA-B	7.190 ± 0.729	9.640 ± 0.497	5.860 ± 0.310	2.920 ± 0.404	1.910 ± 0.356
1994 Jun 29	90.173	VLA-B	10.940 ± 1.103	7.620 ± 0.388	4.240 ± 0.221	2.420 ± 0.359	2.050 ± 0.596
1994 Jul 7	98.027	VLA-B	10.530 ± 1.065	7.340 ± 0.369	4.000 ± 0.207	2.150 ± 0.323	<1.620[a]
1994 Aug 8	130.937	VLA-B	9.410 ± 0.951	5.020 ± 0.262	2.750 ± 0.150	1.480 ± 0.348	<2.400[a]
1994 Aug 22	144.959	VLA-B	11.480 ± 1.155	3.760 ± 0.234	1.930 ± 0.154	1.620 ± 0.476	<1.980[a]
1994 Sep 1	154.753	VLA-B	9.250 ± 1.277	2.073 ± 0.174	1.415 ± 0.139	<1.320[a]	<4.050[a]
1994 Sep 30	183.774	VLA-CnB	10.510 ± 1.196	2.824 ± 0.213	1.530 ± 0.097	<1.830[a]	<2.160[a]

Table 1
(Continued)

Obs. Date	Age (days)	Tel. Config.	S(20 cm) ± rms (mJy)	S(6 cm) ± rms (mJy)	S(3.6 cm) ± rms (mJy)	S(2 cm) ± rms (mJy)	S(1.3 cm) ± rms (mJy)
1994 Oct 13	196.687	VLA-C	<2.841[a]	2.203 ± 0.264	1.117 ± 0.169	<1.140[a]	<1.917[a]
1994 Nov 7	221.513	VLA-C		1.257 ± 0.191	1.220 ± 0.117	<0.990[a]	<2.970[a]
1994 Dec 5	249.708	VLA-D		2.209 ± 0.357	1.024 ± 0.176	<2.220[a]	
1995 Jan 5	280.507	VLA-D				<1.650[a]	
1995 Apr 6	371.173	VLA-D				<1.032[a]	<1.920[a]
1995 Jun 16	442.147	VLA-DnA	2.397 ± 0.253	0.855 ± 0.102			
1995 Oct 6	554.790	VLA-BnA	1.087 ± 0.121	0.503 ± 0.113	0.391 ± 0.072	<0.636[a]	
1996 Jan 12	652.500	VLA-CnB		0.460 ± 0.046		<0.480[a]	
1996 Oct 5	919.847	VLA-DnA	0.580 ± 0.152	0.250 ± 0.071	<0.390[a]		
1999 Jun 13	1900.000	VLA-DnA	<0.222[a]				
2002 Apr 5	2927.000	VLA-A	0.150 ± 0.026				

Note. [a] All upper limits are 3σ.

Table 2
Millimeter Flux Density Measurements for SN 1994I

Obs. Date	Age (days)	Tel.	Flux Density (S) ± rms[a] (mJy)	Frequency (GHz)	Reference
1994 Mar 31	= 0.00				
1994 Apr 5	5.45	OVRO	11.0 ± 0.6	99	Phillips et al. (1994)
1994 Apr 6	6.45	OVRO	<12[b]	218	Phillips et al. (1994)

Notes.
[a] Quoted errors are taken from the original references.
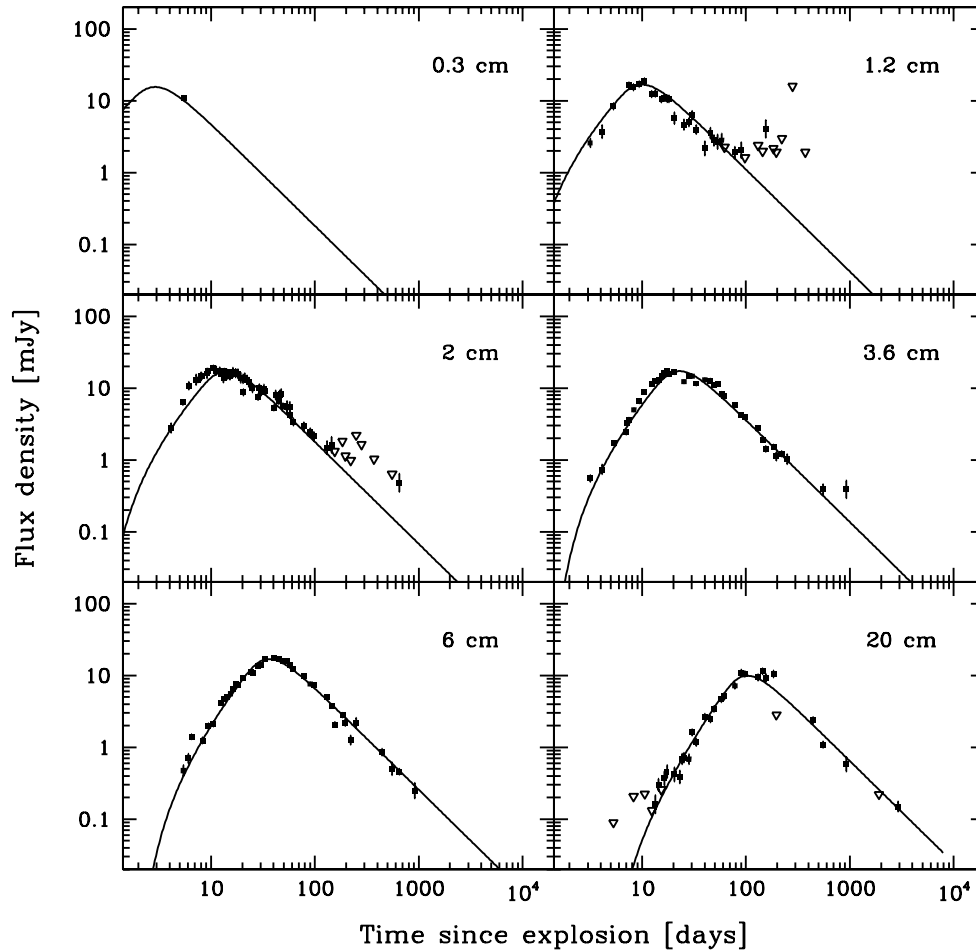[b] All upper limits are 3σ.

Figure 1. Radio light curves for SN 1994I for top left 0.3 cm, top right 1.2 cm, middle left 2 cm, middle right 3.6 cm, lower left 6 cm, and lower right 20 cm. The lines on all figures represent the best-fit model as described in the text with the parameters listed in Table 4.

Table 3
VLA Calibrator Flux Density Measurements[a]

| Obs. Date	S(20 cm) (mJy)	S(6 cm) (mJy)	S(3.6 cm) (mJy)	S(2 cm) (mJy)	S(1.3 cm) (mJy)
1994 Apr 3			0.539[b]		0.338[b]
1994 Apr 4			1.014[c]	0.953[c]	0.830[c]
1994 Apr 5	0.904	1.038	1.014	0.953	0.830
1994 Apr 6		1.020[c]			
1994 Apr 7			0.994	0.959[c]	0.880[c]
1994 Apr 8	0.899[c]	1.025[c]	1.000[c]	0.954[c]	0.875[c]
1994 Apr 9		1.040[c]	1.019[c]	0.980[c]	0.910[c]
1994 Apr 10	0.894	1.013	0.987	0.956	0.920
1994 Apr 12	0.887[c]	1.006[c]	0.974[c]	0.940[c]	0.864[c]
1994 Apr 13	0.884	1.017	0.993	0.955	0.865
1994 Apr 14	0.875[c]	1.026	1.027[c]	0.976[c]	
1994 Apr 15	0.875[c]	1.017[c]	1.029[c]	0.993[c]	0.839[c]
1994 Apr 16	0.875[c]	1.017[c]	1.029[c]	0.993[c]	0.839[c]
1994 Apr 17	0.875[c]	1.060[c]	1.032[c]	0.976[c]	0.810[c]
1994 Apr 18		0.984	0.963	0.930	0.901
1994 Apr 20	0.875[c]	1.005[c]	0.964[c]	0.918[c]	0.773
1994 Apr 23	0.875[c]				
1994 Apr 24	0.875[c]	1.015[c]			
1994 Apr 25	0.904	1.015	0.946		0.689
1994 Apr 28	0.866	0.995	0.937	0.881	0.683
1994 Apr 30	0.887[c]	0.993[c]	0.958[c]	0.890[c]	0.792[c]
1994 May 3	0.905	0.992	0.940		0.900
1994 May 10	0.890	0.946	0.930	0.859	0.846
1994 May 15	0.899	0.983	0.949	0.900	0.816
1994 May 19	0.868	0.948	0.920	0.830	0.764
1994 May 23		0.986	0.933	0.863	0.797
1994 May 28	0.872	0.976	0.939	0.878	0.822
1994 Jun 1	0.894	0.996	0.963	0.874	0.905
1994 Jun 17	0.894	0.991	0.957	0.875	0.793
1994 Jun 29	0.883	0.958	0.918	0.829	0.786
1994 Jul 7	0.882	0.927	0.885	0.783	0.753
1994 Aug 8	0.881	0.912	0.879	0.846	0.827
1994 Aug 22	0.926	0.863	0.784	0.635	0.633
1994 Sep 1	0.906[c]	0.852[c]	0.807[c]	0.657	0.665
1994 Sep 30	0.885	0.831	0.830	0.654	0.528
1994 Oct 13	0.840[c]	0.834[c]	0.822[c]	0.705[c]	0.610[c]
1994 Nov 7		0.826	0.812	0.755	0.693
1994 Dec 5		0.832	0.782	0.680	
1995 Jan 5				0.726	
1995 Apr 6				0.697	0.634
1995 Jun 16	0.760	0.764			
1995 Oct 6	0.705	0.750	0.738	0.702	
1996 Jan 12		0.726		0.697	
1996 Oct 5	0.622	0.775	0.792		
1999 Jun 13	0.498				
2002 Apr 5	0.537[d]				

Notes.
[a] Unless otherwise noted, the flux density measurements are for J1418+546.
[b] Flux density measurements are for J1415+463.
[c] Interpolated from nearby measurements.
[d] Flux density measurement is for 1327+434.

Table 4
Best-fit Parameters for SN 1994I and Comparison with SN 1993J

Parameter	SN 1994I	SN 1993J[a]
K_1	4.78×10^3	4.8×10^3
α	-1.22	-0.81
β	-1.42	-0.73
K_2	3.0×10^1	1.6×10^2
δ	$\equiv -3.00^{\rm b}$	-1.88
K_3	$\equiv 0^{\rm b}$	4.3×10^5
δ'	$\cdots$	-2.83
K_4	4.55×10^{-2}	$\equiv 0$
K_5	6.90×10^5	2.62×10^3
δ''	-4.08	-2.05
K_6	9.96×10^3	$\equiv 0$
δ'''	-2.63	$\cdots$
Distance (Mpc)	8.9	3.63
Date of explosion (t_0)	1994 Mar 31	1993 Mar 28
Time to $S_{\rm 6\ cm\ peak}$ (days)	34.4	133
$S_{\rm 6\ cm\ peak}$ (mJy)	16.2	96.9
$L_{\rm 6\ cm\ peak}$ (erg s^{-1} Hz^{-1})	1.5×10^{27}	1.5×10^{27}
$\dot{M}$ ($M_\odot$ yr^{-1})	$> 1.4 \times 10^{-4c}$	0.5–5.9×10^{-6d}

Notes.
[a] Weiler et al. (2007).
[b] Adopted. Because the amount of thermal material surrounding SN 1994I is so low, it is not possible to determine δ and K_3 from the data fitting, and nominal values were adopted.
[c] Under the assumption of a Wolf–Rayet progenitor; see Section 4.6.
[d] Weiler et al. (2007) found that the mass-loss rate from SN 1993J increased from $\sim 5.4 \times 10^{-7}$ $M_\odot$ yr^{-1} at the time of shock breakout to $\sim 5.9 \times 10^{-6}$ $M_\odot$ yr^{-1} around day ~ 3100 (~ 8000 yr before explosion).
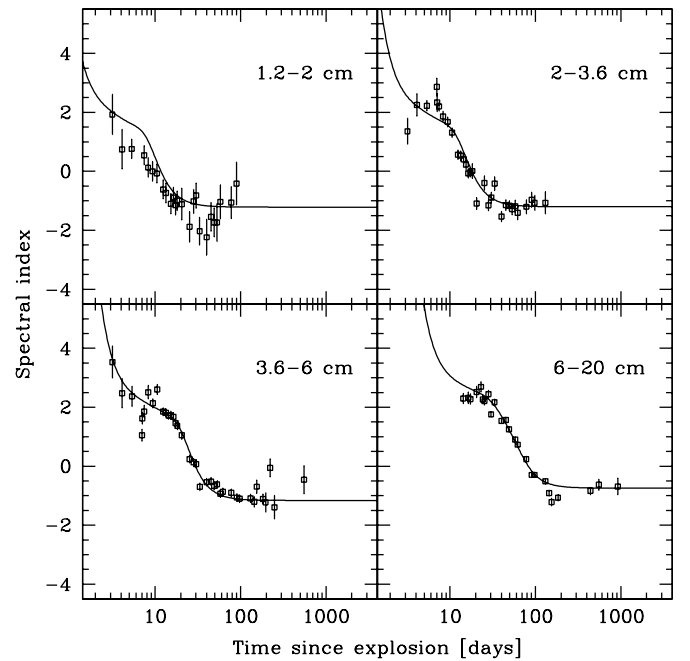
Figure 2. Spectral index evolution for SN 1994I for top left 1.2–2 cm, top right 2–3.6 cm, lower left 3.6–6 cm, and lower right 6–20 cm. The lines on all figures represent the best-fit model as described in the text with the parameters listed in Table 4.

for four pairs of bands (1.2–2 cm, 2–3.6 cm, 3.6–6 cm, and 6–20 cm). The parameters listed in Table 4 from the best-fit light curves allow calculation of the model spectral index evolution curves and these are also shown in Figure 2. At the earliest times, the observed spectral indices exceed the maximum value spectral index ($\alpha = 2.5$) possible for a purely synchrotron self-absorption (SSA) source, suggesting that at least some thermal absorption is present in SN 1994I.

The overall model fits to the spectral index evolution are quite good, with the only exception being the model 1.2–2 cm

spectral index at early times, which is systematically higher than the observed values. This deviation, which was found also for the case of SN 1993J (Weiler et al. 2007), suggests that, at the highest frequencies, the intrinsic radio spectrum has a somewhat
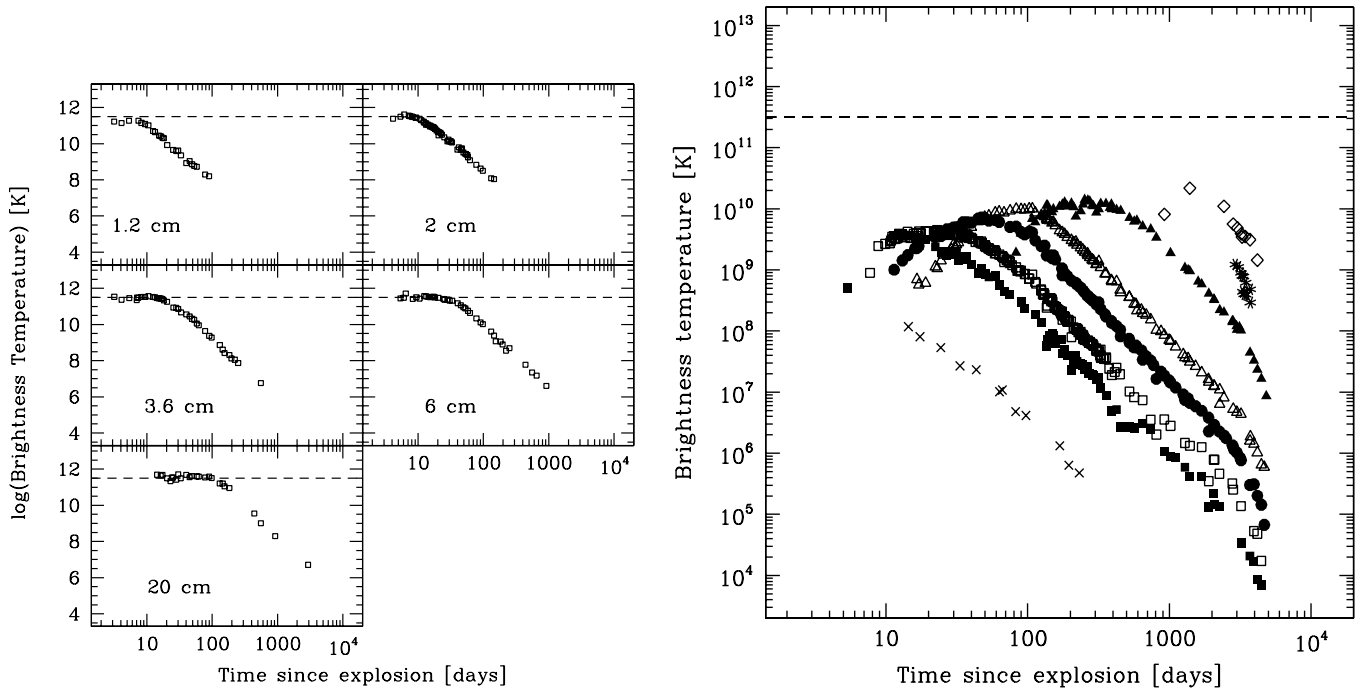
Figure 3. Left: the brightness temperature (T_B) evolution, uncorrected for thermal absorption, for SN 1994I for top left 1.2 cm, top right 2 cm, middle left 3.6 cm, middle right 6 cm, and lower left 20 cm; right: the brightness temperature (T_B) evolution, uncorrected for thermal absorption, for SN 1993J (Weiler et al. 2007) for, from left to right, 0.3 cm (cross), 1.2 cm (filled square), 2 cm (open square), 3.6 cm (filled circle), 6 cm (open triangle), 20 cm (filled triangle), 49 cm (star), and 90 cm (open diamond). The horizontal dashed lines in all plots denote the limiting value of $T_B \simeq 3 \times 10^{11}$ K (Kellermann & Pauliny-Toth 1969; Readhead 1994).

flatter spectral index than the best-fit value determined by the longer wavelength data.

2.3. Brightness Temperature

This extensive data set can also be used to estimate the intrinsic brightness temperature of the SN 1994I radio emission which can be derived from the ratio of the observed radio flux density to the solid angle Ω of the emitting region ($T_B \propto S_{obs}/\Omega$).

Since SN 1994I was not radio bright enough, it was not possible to directly measure its angular size by means of very long baseline interferometry observations, as had been possible for SN 1993J (see, e.g., Marcaide et al. 2009, and references therein), but the physical size of the SN shock can be estimated from the optically measured expansion velocity and distance to the SN. For SN 1994I, published expansion velocities at early times range between $\sim$16,500 km s^{-1} (Filippenko et al. 1995; Millard et al. 1999) from the absorption troughs of He I λ10830, through $\sim$20,000 km s^{-1} (Millard et al. 1999) as seen for Si II, up to almost 30,000 km s^{-1}, that is the extent measured by Filippenko et al. (1995) for the blue wing of the He I λ10830 absorption line. We shall adopt a compromise expansion velocity of 20,000 km s^{-1} and, following Immler et al. (2002), we shall assume that it is constant with time. Therefore, the radius r of the emitting region can be estimated as

$$r = 1.73 \times 10^{14}(t/1 \text{ day}) \text{ cm} \qquad (2)$$

which, for an adopted distance D to SN 1994I of 8.9 Mpc, gives an angular size of

$$\theta = 1.29(t/1 \text{ day}) \, \mu\text{as} \qquad (3)$$

and an estimated brightness temperature of

$$T_B = 3.5 \times 10^{11} S_{obs}(\text{mJy})\lambda^2(t/1 \text{ day})^{-2} \text{ K}. \qquad (4)$$

The resulting brightness temperature evolution is shown in Figure 3 (left). The corresponding brightness temperature evolution curves for SN 1993J from Weiler et al. (2007) are also shown in Figure 3 (right).

From these brightness temperature estimates, we can constrain the value of external absorption due to a presupernova stellar wind by requiring that T_B not exceed the limit of $\sim$3 × 10^{11} K (Kellermann & Pauliny-Toth 1969; Readhead 1994) where the radio emission is quenched by inverse-Compton scattering. This implies that any value of K_2 (see Section 3.1) higher than $\sim$30 would yield T_B curves in strong disagreement with such a physical requirement and puts an upper limit on the amount of external thermal absorption by a presupernova mass loss in a dense stellar wind.

3. RADIO SUPERNOVA MODELS

3.1. Parameterized Model

Weiler et al. (1986) discuss the common properties of RSNe, including non-thermal synchrotron emission with high brightness temperature, turn-on delay at longer wavelengths, power-law decline with index β after maximum, and spectral index α (S $\propto \nu^{+\alpha}$) asymptotically decreasing to an optically thin value. Weiler et al. (1986, 1990) have shown that the "mini-shell" model of Chevalier (1982a, 1982b), with modifications by Weiler et al. (1990), adequately describes previously known RSNe. In this model, the relativistic electrons and enhanced magnetic fields necessary for synchrotron emission are generated by the SN shock interacting with a relatively high density circumstellar envelope which has been ionized and heated by the initial UV/X-ray flash. Figure 4 (taken from Weiler et al. 2002) shows a, not to scale, greatly simplified cartoon of the vicinity of a supernova explosion. This dense cocoon is presumed to have been established by a constant mass-loss ($\dot{M}$) rate,
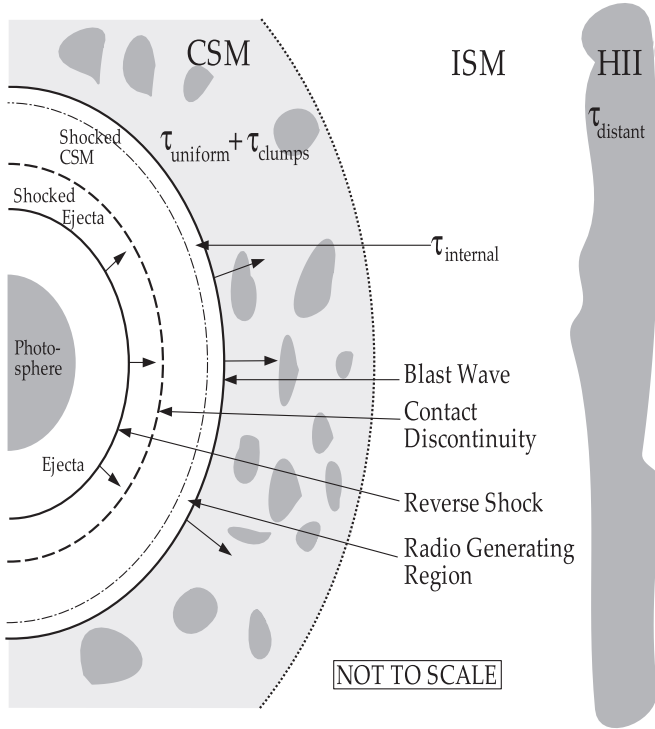
Figure 4. Cartoon (taken from Weiler et al. (2002)), not to scale, of the supernova and its shocks, along with the stellar wind established CSM, the interstellar medium (ISM), and more distant ionized hydrogen (H II) absorbing gas. The radio emission is thought to arise near the blast wave front. The expected locations of the several absorbing terms in Equations (5)–(12) are illustrated.

constant velocity (w) wind (i.e., $\rho_{CSM} \propto r^{-2}$) from a massive ($>8\,M_\odot$) stellar progenitor or companion. This ionized CSM can also be the source of initial thermal absorption (free–free absorption, FFA) although Chevalier (1998) has suggested that non-thermal, SSA may be a significant source of absorption in the early phases of some RSNe. For the case of FFA, the rapid rise in radio flux density results from the shock overtaking progressively more of the wind matter, leaving less of it along the line of sight to the observer to absorb the more slowly decreasing synchrotron emission from the shock region. In the case of SSA, the non-thermal absorption decreases as the emitting region expands and decreases in density. Montes et al. (1997) also allow for the possibility of intervening H II along the line of sight to the RSN, providing a constant thermal absorption of the radio emission.

To parameterize the basic characteristics of RSNe, we adopt the most recent RSN discussion of Weiler et al. (2002) and Sramek & Weiler (2003)[8] and illustrate the regions of the supernova being parameterized in a cartoon shown in Figure 4 from, e.g., Weiler et al. (2002):

$$S(\text{mJy}) = K_1 \left(\frac{\nu}{5\,\text{GHz}}\right)^\alpha \left(\frac{t - t_0}{1\,\text{day}}\right)^\beta e^{-\tau_{\text{external}}}$$
$$\times \left(\frac{1 - e^{-\tau_{\text{CSM}_{\text{clumps}}}}}{\tau_{\text{CSM}_{\text{clumps}}}}\right)\left(\frac{1 - e^{-\tau_{\text{internal}}}}{\tau_{\text{internal}}}\right) \quad (5)$$

with

$$\tau_{\text{external}} = \tau_{\text{CSM}_{\text{homogeneous}}} + \tau_{\text{distant}}, \quad (6)$$

---

[8] Even though this model has been previously described in papers such as the references given above, we list it again for completeness, for the reader's convenience, and for explanation of the parameters listed in Table 4.

where

$$\tau_{\text{CSM}_{\text{homogeneous}}} = K_2 \left(\frac{\nu}{5\,\text{GHz}}\right)^{-2.1} \left(\frac{t - t_0}{1\,\text{day}}\right)^\delta \quad (7)$$

$$\tau_{\text{distant}} = K_4 \left(\frac{\nu}{5\,\text{GHz}}\right)^{-2.1} \quad (8)$$

and

$$\tau_{\text{CSM}_{\text{clumps}}} = K_3 \left(\frac{\nu}{5\,\text{GHz}}\right)^{-2.1} \left(\frac{t - t_0}{1\,\text{day}}\right)^{\delta'} \quad (9)$$

with K_1, K_2, K_3, and K_4 determined from fits to the data and corresponding, formally, to the flux density (K_1), homogeneous (K_2, K_4), and clumpy or filamentary (K_3) FFA at 5 GHz one day after the explosion date t_0. The terms $\tau_{\text{CSM}_{\text{homogeneous}}}$ and $\tau_{\text{CSM}_{\text{clumps}}}$ describe the attenuation due to local, homogeneous FFA CSM and clumpy or filamentary FFA CSM, respectively, that are near enough to the SN progenitor that they are altered by the rapidly expanding SN blast wave. The $\tau_{\text{CSM}_{\text{homogeneous}}}$ FFA is produced by an ionized medium that completely covers the emitting source ("homogeneous external absorption"), and the $(1 - e^{-\tau_{\text{CSM}_{\text{clumps}}}})\tau_{\text{CSM}_{\text{clumps}}}^{-1}$ term describes the attenuation produced by an inhomogeneous FFA medium ("clumpy absorption;" see Natta & Panagia 1984, for a more detailed discussion of attenuation in inhomogeneous media). The τ_{distant} term describes the attenuation produced by a homogeneous FFA medium which completely covers the source but is so far from the SN progenitor that it is not affected by the expanding SN blast wave and is consequently constant in time. All external and clumpy absorbing media are assumed to be purely thermal, singly ionized gas which absorbs via FFA with frequency dependence $\nu^{-2.1}$ in the radio. The parameters δ and δ' describe the time dependence of the optical depths for the local homogeneous and clumpy or filamentary media, respectively.

Since it is physically realistic and is needed in some RSNe where radio observations have been obtained at early times and high frequencies, Equation (5) also includes the possibility for an internal absorption term.[9] This internal absorption (τ_{internal}) term may consist of two parts—SSA ($\tau_{\text{internal}_{\text{SSA}}}$), and thermal FFA ($\tau_{\text{internal}_{\text{FFA}}}$) due to ionized gas mixed with non-thermal emission.

$$\tau_{\text{internal}} = \tau_{\text{internal}_{\text{SSA}}} + \tau_{\text{internal}_{\text{FFA}}} \quad (10)$$

$$\tau_{\text{internal}_{\text{SSA}}} = K_5 \left(\frac{\nu}{5\,\text{GHz}}\right)^{\alpha - 2.5} \left(\frac{t - t_0}{1\,\text{day}}\right)^{\delta''} \quad (11)$$

$$\tau_{\text{internal}_{\text{FFA}}} = K_6 \left(\frac{\nu}{5\,\text{GHz}}\right)^{-2.1} \left(\frac{t - t_0}{1\,\text{day}}\right)^{\delta'''} \quad (12)$$

with K_5 corresponding, formally, to the internal, non-thermal ($\nu^{\alpha - 2.5}$) SSA and K_6, corresponding, formally, to the internal thermal ($\nu^{-2.1}$) FFA mixed with non-thermal emission, at 5 GHz one day after the explosion date t_0. The parameters δ'' and δ''' describe the time dependence of the optical depths for the SSA and FFA internal absorption components, respectively.

---

[9] Note that for simplicity an internal absorber attenuation of the form $((1 - e^{-\tau_{\text{CSM}_{\text{internal}}}})/\tau_{\text{CSM}_{\text{internal}}})$, which is appropriate for a plane-parallel geometry, is used instead of the more complicated expression (e.g., Osterbrock 1974) valid for the spherical case. The assumption does not affect the quality of the analysis because, to within 5% accuracy, the optical depth obtained with the spherical case formula is simply three-fourths of that obtained with the plane-parallel slab formula.

Application of this basic parameterization has been shown to be effective in describing the physical characteristics of the presupernova system, its CSM, and its final stages of evolution before explosion for objects ranging from the two decades of monitoring the complex radio emission from SN 1979C (Montes et al. 2000), through the unusual SN 1998bw (GRB 980425; Weiler et al. 2001a), to most recent γ-ray bursters/Type Ib/c SNe (Weiler et al. 2002, 2003).

4. DISCUSSION

4.1. Application of Models to SN 1994I

As was clearly demonstrated by Weiler et al (2007) for the case of SN 1993J, in order to obtain a meaningful representation of radio observations of a supernova, a model must be able to account simultaneously for three different aspects, namely, (1) the light curves measured at several epochs and in several distinct radio bands, (2) the corresponding spectral indices computed for pairs of bands at adjacent frequencies, and (3) the brightness temperatures, which at all times should be lower than the well-established limit of 3×10^{11} K (Kellermann & Pauliny-Toth 1969; Readhead 1994).

4.2. SN 1994I Radio Light Curves

We have excellent time coverage of the radio emission from SN 1994I at 5 frequencies, from 22 GHz down to 1.4 GHz. That enables us to make a detailed study of its radio properties. In particular, the rising branch of the light curve at early times, where absorption ($\tau \gg 1$) is still important, is well defined in all five main bands. Also, the flux density evolution is well characterized by a power-law decay at late times, in the optically thin phases. Therefore, we are in an excellent position to identify the main processes operating in this source and determine their parameters. Actually, the best-fit curves as described by the parameters in Table 4 and shown in Figure 1 agree quite well with the observations, with an overall $\chi^2 = 4.42$ per degree of freedom.

From this rather good parameterization of the radio emission from SN 1994I, we conclude that the radio light curves are not well described by a purely thermal absorption model such as that given by Equations (5)–(9). In particular, the requirement for non-zero K_5 and K_6 parameter values implies the existence of significant SSA. In fact, the early optical depth is dominated almost entirely by the SSA (K_5) component, and the FFA component (K_6) makes a significant contribution only as the emission becomes more optically thin and the brightness temperature begins to drop. As predicted by Chevalier (1998), there does not appear to be a highly-structured, thick CSM present since there is no need for a large K_2 or non-zero K_3 term. The necessity of a K_4 term (i.e., thermal absorption by foreground H II gas; see Section 4.5) is consistent with recent deep 20 cm observations that indicate diffuse radio emission from the host galaxy in the region near the supernova (Maddox et al. 2007). Further evidence for substantial amounts of H II gas is provided by the Hα emission detected on *HST* images of the immediate vicinity of SN 1994I (Maddox 2006; Maddox et al. 2007).

It is interesting to note that SN 1994I shows a dip around day 27 in its flux density at centimeter wavelengths (frequencies from 4.9 GHz to 22 GHz). While less pronounced than that noted for the unusual Type Ib/c SN 1998bw, which is related to the γ-ray burster GRB 980425, it occurs on a similar timescale (see Kulkarni et al. 1998, and

http://www.narrabri.atnf.csiro.au/public/grb/grb980425/). This early "dip" followed by "re-brightening" for SN 1998bw has variously been explained as due to a slowing and re-energization of the SN blast wave (Li & Chevalier 1999) or, more likely, as structure in the circumstellar absorbing material (Weiler et al. 2001a, 2001b).

Considering the light curves shown in Figure 1 in more detail, even though the fitted model provides a good representation the agreement is never quite perfect, mostly because the model is rather simplified and also because there may be systematic deviations from our basic assumptions. In order to analyze the residuals between the model and the observations, we express them as logarithms of the ratios of observed to model fluxes and plot them in Figure 5 (left). A similar analysis helped us in other RSNe to reveal unsuspected features such as a periodic flux modulation for SN 1979C (Weiler et al. 1992; Schwarz & Pringle 1996) possibly due to the presence of a companion, as well as evidence for interacting winds in SN 2001ig (Ryder et al. 2004).

The residuals for SN 1994I are displayed separately for individual bands in Figure 5 (left) and merged in a single plot in Figure 5 (right). As expected, they show scatter inherent to non-negligible measurement errors and to a simplified description of a complicated phenomenon. However, a systematic feature is apparent, essentially with the same timing and comparable amplitudes, at all bands. In particular, in Figure 5 (right) we can see a somewhat broad trough, with an apparent local minimum, which is about 0.2 deep in the logarithm and occurring $\sim$27 days after explosion. This trough extends from $\sim$10 up to $\sim$55 days after explosion. Since this local minimum is present at all frequencies with similar amplitude, it must represent a genuine decrease in the intrinsic emission rather than being the result of additional, temporary absorption along the line of sight. In a spherically symmetric model it would correspond to a temporary decrease of the average density of the CSM by $\sim$0.1 in the logarithm of the ratio, or a factor of $\sim$0.8 decrease in the CSM density, with a duration of $\sim$45 days.

Although a temporary decrease in the mass-loss rate from the presupernova star cannot be ruled out, we feel it worthwhile to also consider a model in which the SN 1994I progenitor was a Wolf–Rayet (W-R) star in a wide binary system whose companion was also an early-type star (most likely a B-type star on the main sequence). Such a binary system could create non-spherical CSM density structures by the interacting winds of the system stars (see, e.g., Schwarz & Pringle 1996). If such were the case, for SN 1994I the observed minimum in the residuals would correspond to a separation between the two stars of $\sim$4.7 × 10^{15} cm or $\sim$310 AU (see also SN 1979C (Weiler et al. 1992; Schwarz & Pringle 1996) where the radio emission modulation is possibly due to the presence of a companion, as well as evidence for interacting winds in SN 2001ig (Ryder et al. 2004)).

4.3. SN 1994I Spectral Index Evolution

Examination of the spectral index evolution in Figure 2 shows three things: (1) the model listed in Table 4 generally describes the spectral index evolution quite well except at 1.2–2 cm. Apparently, at higher frequencies the model is beginning to fail. (2) The spectral index evolution, particularly at the first part at 3.6–6 cm, requires some (small) amount of thermal absorption since SSA can never generate a spectral index exceeding +2.5. (3) There is no evidence for systematic spectral index change of the emission within the available observations. While
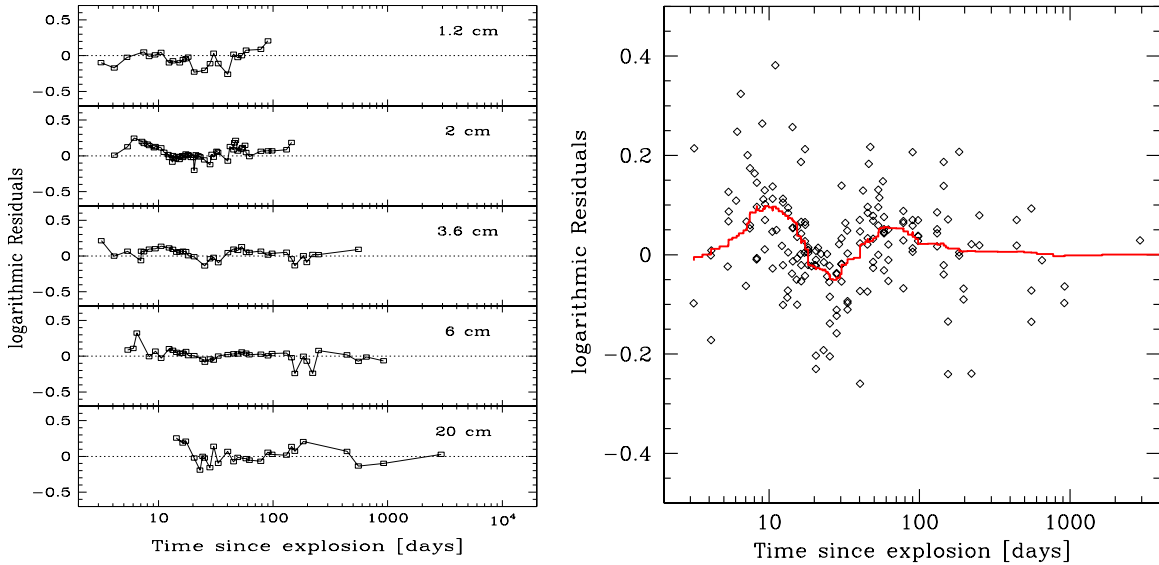
Figure 5. Left: log of the deviations of the ratio of observed to model flux densities for SN 1994I for the best-fit model listed in Table 4 from 1.2 cm (top) to 20 cm (bottom); right: composite of the deviations at all wavelengths shown on the left, with a smoothed curve added to guide the eye.

(A color version of this figure is available in the online journal.)

short-term fluctuations of the spectral index cannot be ruled out, none appear to occur at the same epoch at all frequencies.

4.4. Brightness Temperature

Figure 3 shows the estimated brightness temperatures for each frequency versus time for SNe 1994I (left) and 1993J (right; from Weiler et al. 2007). While the precise temperature measurements depend on the distance used and the assumed (or, for SN 1993J, measured) shock wave speed, it is clear that the two plots have a systematic difference at early times. In the case of SN 1994I, the temperatures for each frequency appear to remain approximately constant near the maximum possible value of 3×10^{11} K (see Section 2.3) until the source becomes optically thin. However, the measured brightness temperatures for SN 1993J at the earliest times increase for each frequency until the emission becomes optically thin. This is evidence that the dominant absorption mechanism is different between these two SNe, with the primary absorption mechanism for SN 1993J not directly related to the emission mechanism (i.e., external thermal electrons), while the primary absorption mechanism for SN 1994I is physically associated with the emission mechanism (i.e., synchrotron electrons). This simple comparison makes it clear that SSA is dominant in SN 1994I at early times while, as demonstrated by Weiler et al. (2007), SN 1993J requires significant contributions to the early absorption from *both* FFA and SSA. Thus, SN 1994I is the first observed RSN to clearly demonstrate the need for an SSA dominated component to model its radio light curves.

4.5. External Distant Absorption

The parameter K_4 (see Section 3.1) is interpreted as being due to a constant amount of ionized material between us and SN 1994I that is sufficiently far from the SN to be unaffected by the expanding shock wave. It is related to the emission measure (EM) of this intervening ionized hydrogen by Equation (1-223) of Lang (1980) so that

$$\mathrm{EM} = 8.93 \times 10^7 K_4 (T_e/10^4 \, \mathrm{K})^{1.35} \, \mathrm{pc \, cm}^{-6}, \qquad (13)$$

where T_e is the electron temperature of the ionized absorbing medium. Thus, the value for K_4 in Table 4 implies a presence along the line of sight to SN 1994I of ionized hydrogen with an emission measure of EM $\simeq 4.1 \times 10^6 (T_e/10^4 \, \mathrm{K})^{1.35}$ pc cm^{-6}.

Similar to the case of SN 1978K (Montes et al. 1997; Chu et al. 1999) this thermal absorption is likely to be due to an intervening H II region and not part of the matter from the presupernova mass-loss wind. Most H II regions with an EM higher than $\sim 10^6$ pc cm^{-6} are known to be rather compact sources (see, e.g., Wilson et al. 1970; Reifenstein et al. 1970); for example, the Orion Nebula has an average EM of 1.8×10^6 pc cm^{-6} and a diameter of ~ 2 pc (Allen 1973). If we adopt a similar diameter of ~ 2 pc for this H II region presumed to be along the line of sight to SN 1994I, we derive an average electron density of 2×10^3 pc cm^{-6} and a total mass of the ionized gas of $M(\mathrm{H \, II}) \simeq 250 \, M_\odot$. The volume EM is then $n_e^2 V \simeq 5.1 \times 10^{62}$ cm^{-3}, which implies a steady source of ionizing radiation of $N_L \simeq 1.3 \times 10^{50}$ Lyman-continuum photons s^{-1}. Such a flux is higher than that provided even by a bright O-type star (see, e.g., Panagia 1973) and suggests the presence of a young, compact star cluster in the foreground of SN 1994I.

In order not to make the projection of such a powerful cluster in front of SN 1994I too geometrically improbable, the cluster should be spatially close to the supernova itself; say, separated by no more than ~ 3 pc, which would give a probability of chance projection of $\sim 3\%$. This then implies that the progenitor of SN 1994I may have been a member of that cluster and, by association, was a massive star.

4.6. Pre-supernova Mass-loss Rate

The best-fit value for the parameter K_2 (see Section 3.1) is related to the density of a presupernova stellar wind. If the density distribution in the CSM around SN 1994I is proportional to r^{-2}, as appropriate for a constant mass-loss rate, constant velocity progenitor wind confirmed by Immler et al. (2002), our measurement of $K_2 = 30$ in Table 4 corresponds to a CSM external thermal absorption as a function of time of

$$\tau(\lambda, t) = 0.35 \lambda^{-2.1} (t/1 \, \mathrm{day})^{-3}. \qquad (14)$$

9

Assuming for the moment that the progenitor star for SN 1994I was a red supergiant (RSG), inserting Equation (14) into Equation (16) of Weiler et al. (1986), adopting an electron temperature of $T_e = 20,000$ K for the absorbing CSM gas, and assuming a wind velocity for this suggested RSG progenitor of $w = 10$ km s^{-1}, we obtain a mass-loss rate of

$$\dot{M} = 1.8 \times 10^{-7}(v_s/20,000 \, \text{km s}^{-1})^{1.5}(w/10 \, \text{km s}^{-1})$$
$$\times (T_e/20,000 \, \text{K})^{0.68} \, M_\odot \, \text{yr}^{-1}. \quad (15)$$

This estimate of $\dot{M}$ is much lower than the estimate of $1.1 \times 10^{-5}(w/10 \, \text{km s}^{-1}) \, M_\odot \, \text{yr}^{-1}$ obtained by Immler et al. (2002) from their analysis of the SN 1994I X-ray emission data.

Clumping of the CSM (or a systematic deviation from spherical symmetry) might provide a simple explanation for this apparent discrepancy if most of the ionized gas is present in the form of large, isolated structures. In such a case, the mass-loss rate derived from the X-ray emission, which is integrated over the whole CSM, would be much higher than that estimated from the radio absorption because the latter arises only from the material along the line of sight which may not intercept any dense clumps in the CSM. Indeed, in deriving their $\dot{M}$ estimate Immler et al. (2002) assumed that the CSM was both uniform and spherically symmetric. If such appreciable clumping is present, the average density of the emitting material could be grossly underestimated for radio measurements of absorption along the line of sight by a factor equal to the square root of the clumping factor. The X-ray estimated mass-loss rate (proportional to the ratio of the X-ray luminosity to the average density) would then be overestimated by the same factor. Conversely, the radio absorption-based estimate would provide only a lower limit to the true mass-loss rate. Thus, with a suitable selection of the clumping factor such a large difference between the radio and X-ray estimates could be accounted for without abandoning the RSG progenitor assumption. For example, if we take a "compromise" value of

$$\sqrt{\dot{M}(\text{radio}) \times \dot{M}(\text{X-ray})} \simeq 1.4 \times 10^{-6}(w/10 \, \text{km s}^{-1}) \, M_\odot \, \text{yr}^{-1} \quad (16)$$

to be appropriate for SN 1994I progenitor's wind, the clumping factor would be $\sim$40 and the fraction of mass in the diffuse component $\sim$15%.

On the other hand, if the progenitor of SN 1994I was *not* an RSG star but a W-R star, as has been suggested for Type Ib/c SNe by many authors (see, e.g., van den Bergh 1988; Gal-Yam et al. 2007; Smartt 2009; and references therein), the W-R progenitor would have a much higher wind speed ($>10^3$ km s^{-1}; see, e.g., Willis 1996), as opposed to $\sim$10 km s^{-1} for an RSG star. Thus, a W-R progenitor would revise the above estimate of the presupernova mass-loss rate from Equation (16) upward to $\dot{M} > 1.4 \times 10^{-4} \, M_\odot \, \text{yr}^{-1}$, a mass-loss rate that is quite possible for a W-R star toward the end of its evolution (see, e.g., Willis 1996).

5. CONCLUSIONS

We present detailed radio observations of SN 1994I at multiple wavelengths from a few days to more than eight years after explosion. Although there have been many radio observations of Type Ib/c supernovae since SN 1994I, SN 1994I remains the best-studied and most heavily sampled example of the class. Also, even though observations since those of SN 1994I have indicated that SSA can play a role in the early

radio light curves of supernovae that have relatively low density circumstellar matter, such as Type Ib/c and Type IIb, SN 1994I was the first example that was so well sampled early enough that such a conclusion was inescapable. Also, as seen in other RSNe (see Section 4.2) this low-density circumstellar thermal material in SN 1994I may be irregularly distributed as discussed in Section 4.6.

As with previous detailed observations of the radio emission from supernovae, there is no sign of systematic spectral index evolution with time. However, a changing spectral index with frequency, rather than with time, is a distinct possibility, with the highest observed frequencies perhaps indicating a somewhat flatter spectral index.

As has been noted in the few other RSNe which have been sufficiently well studied, the radio light curves, even though their general properties evolve smoothly and are well described by existing models, show significant "bumps and wiggles." SN 1994I shows a significant local "dip" between $\sim$10 and $\sim$55 days after explosion that is interpreted as a temporary decrease in the average density of the circumstellar medium, perhaps implying the origin of SN 1994I in an exploding W-R star in a wide binary system with an early-type stellar companion, although changing mass-loss rate from the progenitor star cannot be ruled out.

The usual scenario for core-collapse (Type Ib/c and Type II) supernovae is that the progenitor was an RSG. However, based on the information available from these new observations, it appears that a W-R star undergoing a period of very high mass-loss rate is the most likely progenitor star for SN 1994I.

REFERENCES

Allen, C. W. 1973, (3rd ed., London: Univ. London Athlone Press)
Armus, L., & Mazzarella, J. M. 1994, IAU Circ., 5961
Berger, E., Kulkarni, S. R., Frail, D. A., & Soderberg, A. M. 2003a, ApJ, 599, 408
Berger, E., Soderberg, A. M., Frail, D. A., & Kulkarni, S. R. 2003b, ApJ, 587, L5
Chevalier, R. A. 1982a, ApJ, 259, 302
Chevalier, R. A. 1982b, ApJ, 259, L85
Chevalier, R. A. 1998, ApJ, 499, 810
Chu, Y.-H., Caulet, A., Montes, M. J., et al. 1999, ApJ, 512, L51
Clocchiatti, A., Brotherton, M., Harkness, R. P., & Wheeler, J. C. 1994, IAU Circ., 5972
Feldmeier, J. J., Ciardullo, R., & Jacoby, G. H. 1997, ApJ, 479, 231
Filippenko, A. V., Barth, A. J., Matheson, T., et al. 1995, ApJ, 450, L11
Filippenko, A., Matheson, T., & Barth, A. 1994, IAU Circ., 5964
Gal-Yam, A., Leonard, D. C., Fox, D. B., et al. 2007, ApJ, 656, 372
Goss, W. M., Allen, R. J., Ekers, R. D., & de Bruyn, A. G. 1973, Nature, 243, 42
Gottesman, S. T., Broderick, J. J., Brown, R. L., Balick, B., & Palmer, P. 1972, ApJ, 174, 383
Immler, S., Pietsch, W., & Aschenbach, B. 1998, A&A, 336, L1
Immler, S., Wilson, A. S., & Terashima, Y. 2002, ApJ, 573, L27
Kellermann, K. I., & Pauliny-Toth, I. I. K. 1969, ApJ, 155, L71
Kirshner, R. 1994, IAU Circ., 5981
Kulkarni, S. R., Frail, D. A., Wieringa, M. H., et al. 1998, Nature, 395, 663
Lang, K. R. 1980, in Astrophysical Formulae. A Compendium for the Physicist and Astrophysicist, XXIX, 783 (Berlin: Springer), 47

Lewin, W. H. G., Zimmermann, H.-U., & Pietsch, W. 1994, IAU Circ., 6019
Li, Z.-Y., & Chevalier, R. A. 1999, ApJ, 526, 716
Maddox, L. A. 2006, PhD thesis, Univ. Oklahoma (Publication Number: AAT 3222155. Source: DAI-B 67/06, Dec 2006)
Maddox, L. A., Cowan, J. J., Kilgard, R. E., Schinnerer, E., & Stockdale, C. J. 2007, AJ, 133, 2559
Marcaide, J. M., Martí-Vidal, I., Alberdi, A., et al. 2009, A&A, 505, 927
Millard, J., Branch, D., Baron, E., et al. 1999, ApJ, 527, 746
Minkowski, R. 1941, PASP, 53, 224
Montes, M. J., Weiler, K. W., & Panagia, N. 1997, ApJ, 488, 792
Montes, M. J., Weiler, K. W., Van Dyk, S. D., et al. 2000, ApJ, 532, 1124
Montes, M. J., Van Dyk, S. D., Weiler, K. W., Sramek, R. A., & Panagia, N. 1998, ApJ, 506, 874
Morrison, L. V., & Argyle, R. W. 1994, IAU Circ., 5999
Natta, A., & Panagia, N. 1984, ApJ, 287, 228
Osterbrock, D. E. 1974, Astrophysics of Gaseous Nebulae (San Francisco: Freeman), 82
Panagia, N. 1973, AJ, 78, 929
Panagia, N., Sramek, R. A., & Weiler, K. W. 1986, ApJ, 300, L55
Panagia, N., Van Dyk, S. D., Weiler, K. W., et al. 2006, ApJ, 646, 369
Phillips, M. 1994, IAU Circ., 5966
Phillips, J. A., Chandler, C. J., & Rupen, M. P. 1994, IAU Circ., 5968
Puckett, T., & Armstrong, J. 1994, IAU Circ., 5961
Readhead, A. C. S. 1994, ApJ, 426, 51
Reifenstein, E. C., Wilson, T. L., Burke, B. F., Mezger, P. G., & Altenhoff, W. J. 1970, A&A, 4, 357
Richmond, M. 1994, IAU Circ., 5966
Richmond, M. W., & Filippenko, A. V. 1994, IAU Circ., 5961
Richmond, M. W., Filippenko, A. V., Treffers, R. R., & Van Dyk, S. D. 1994, IAU Circ., 5963
Rodriguez-Pascual, P. M., Monier, R., & Wamsteker, W. 1994, IAU Circ., 5968
Rudy, R., & Dotan, Y. 1994, IAU Circ., 5991
Rupen, M. P., Sramek, R. A., Van Dyk, S. D., Weiler, K. W., & Panagia, N. 1994, IAU Circ., 5963
Ryder, S. D., Sadler, E. M., Subrahmanyan, R., et al. 2004, MNRAS, 349, 1093
Sadler, E. M., Stathakis, R. A., Boyle, B. J., & Ekers, R. D. 1998, IAU Circ., 6901
Sandage, A., & Tammann, G. A. 1974, ApJ, 194, 559
Schmidt, B., Challis, P., & Kirshner, R. 1994, IAU Circ., 5966
Schmidt, B., & Kirshner, R. 1994, IAU Circ., 5962
Schwarz, D. H., & Pringle, J. E. 1996, MNRAS, 282, 1018
Smartt, S. J. 2009, ARA&A, 47, 63
Soderberg, A. M., Chakraborti, S., Pignata, G., et al. 2010, Nature, 463, 513
Soderberg, A. M., Frail, D. A., & Wieringa, M. H. 2004, ApJ, 607, L13
Soderberg, A. M., Kulkarni, S. R., Berger, E., et al. 2005, ApJ, 621, 908
Soderberg, A. M., Nakar, E., Berger, E., & Kulkarni, S. R. 2006, ApJ, 638, 930
Sramek, R. A., Panagia, N., & Weiler, K. W. 1984, ApJ, 285, L59
Sramek, R. A., & Weiler, K. W. 2003, in Supernovae and Gamma-Ray Bursters, ed. K. W. Weiler (Berlin: Springer), 153
Tongue, T., Graham, M., Stanley, M., Truesdell, L., & Westphal, D. 1994, IAU Circ., 5990
Tully, R. B. 1988, Nearby Galaxies Catalog (Cambridge: Cambridge Univ. Press)
van den Bergh, S. 1988, ApJ, 327, 156
van Dyk, S. D., Sramek, R. A., Weiler, K. W., & Panagia, N. 1993, ApJ, 409, 162
Weiler, K. W., Panagia, N., & Montes, M. J. 2001a, ApJ, 562, 670
Weiler, K. W., Panagia, N., & Montes, M. J. 2003, in Supernovae and Gamma-Ray Bursters, ed. K. W. Weiler (Berlin: Springer), 367
Weiler, K. W., Panagia, N., Montes, M. J., & Sramek, R. A. 2002, ARA&A, 40, 387
Weiler, K. W., Panagia, N., & Sramek, R. A. 1990, ApJ, 364, 611
Weiler, K. W., Panagia, N., Sramek, R. A., et al. 2001b, in Proc. Space Telescope Science Institute Symp., Supernovae and Gamma-Ray Bursts: The Greatest Explosions Since the Big Bang, ed. M. Livio, N. Panagia, & K. Sahu (Vol. 13; Cambridge: Cambridge Univ. Press), 198
Weiler, K. W., & Sramek, R. A. 1980, IAU Circ., 3485
Weiler, K. W., Sramek, R. A., Panagia, N., van der Hulst, J. M., & Salvati, M. 1986, ApJ, 301, 790
Weiler, K. W., Van Dyk, S. D., Pringle, J., & Panagia, N. 1992, ApJ, 399, 672
Weiler, K. W., Williams, C. L., Panagia, N., et al. 2007, ApJ, 671, 1959
Willis, A. J. 1996, Ap&SS, 237, 145
Wilson, T. L., Mezger, P. G., Gardner, F. F., & Milne, D. K. 1970, A&A, 6, 364